Enhanced biodegradation of naphthalene by *Pseudomonas* sp. consortium immobilized in calcium alginate beads

Kunal Dutta[1], Sergey Shityakov[2], Ibrahim Khalifa[3,4], Saroj Ballav[1], Debarati Jana[1], Tuhin Manna[1], Monalisha Karmakar[1], Priyanka Raul[1], Kartik Chandra Guchhait[1] and Chandradipa Ghosh[1,*]

[1]Microbiology and Immunology Laboratory, Department of Human Physiology with Community Health, Vidyasagar University, Midnapore -721102, West Bengal, India.

[2]Department of Anaesthesia and Critical Care, University of Würzburg, 97080 Würzburg, Germany.

[3]Food Technology Department, Faculty of Agriculture, 13736 Moshtohor, Benha University, Egypt.

[4]College of Food Science and Technology, Huazhong Agricultural University, Wuhan 430070, PR China.

** Corresponding author:*

Prof. Chandradipa Ghosh
Microbiology and Immunology Laboratory
Department of Human Physiology with Community Health
Vidyasagar University
Midnapore - 721102
West Bengal,
INDIA
Email : ch_ghosh@mail.vidyasagar.ac.in
Phone : +91 3222 276554/555/557 Extn. 450
Fax : +91 3222 275329

Kunal Dutta : orcid.org/0000-0002-0818-8787

Sergey Shityakov : orcid.org/0000-0002-6953-9771

Ibrahim Khalifa : orcid.org/0000-0002-7648-2961

Abstract

Polycyclic aromatic hydrocarbons (PAHs) belong to a large group of organic pollutant which considers as a potential health hazard to living beings. Herein, naphthalene biodegradation potential by free and immobilized *Pseudomonas putida* strain KD10 and *Pseudomonas* sp. consortium were studied. Additionally, naphthalene 1, 2-dioxygenase (*nah*Ac) was sequenced and analyzed, which reveals two altered amino acid residues. However, the altered amino acid residues are not present in the vicinity of the active site. The gas-phase binding free energy (ΔG_{London}) of the mutant variant of naphthalene 1, 2-dioxygenase was -7.10 kcal mol^{-1} which closely resembles the wild type variant. Naphthalene biodegradation rate by *Pseudomonas putida* strain KD10 was 79.12 mg L^{-1} day^{-1} and it was significantly elevated up to 123 mg L^{-1} day^{-1} by the immobilized *Pseudomonas* sp. consortium. The half-life ($t_{1/2}$) for naphthalene biodegradation was 3.1 days with the inhibition constant (k_i), substrate saturation constant (k_s) and maximum specific degradation rate constant (q_{max}) of 1268 mg L^{-1}, 395.5 mg L^{-1} and 0.65 h^{-1}, respectively, for the *Pseudomonas putida* strain KD10. However, the $t_{1/2}$ value was significantly reduced to 2 days along with k_i, k_s and q_{max} values of 1475 mg L^{-1}, 298.8 mg L^{-1} and 0.71 h^{-1}, respectively, by the immobilized *Pseudomonas* sp. consortium. The GC-MS data suggest that KD10 might follow D-gluconic acid mediated meta-cleavage pathway of catechol biodegradation. It is concluded that naphthalene biodegradation performance by immobilized *Pseudomonas* sp. consortium was superior to free or immobilized *Pseudomonas putida* KD10. Microbial consortium immobilization could be a useful tool for water quality management and environmental remediation.

Keywords:

Pseudomonas sp., petroleum wastes, biodegradation, cell immobilization, mutant naphthalene 1, 2-dioxygenase, rigid-flexible molecular docking.

Highlights

- Superior naphthalene biodegradation by *Pseudomonas* sp. consortium immobilized in calcium alginate beads.
- A common mutation prone amino acid stretch inside chain A of naphthalene 1, 2-dioxygenase has been identified.
- A new naphthalene biodegradation pathway by *Pseudomonas putida* strain KD10 has been proposed.

1. Introduction

Polycyclic aromatic hydrocarbons (PAHs) are considered as the potential health hazard for living beings (Kumari et al., 2018). Environmental agencies including US-EPA, European Union, Environment-Canada, registered PAH as the priority pollutants that require immediate human intervention (Wang et al., 2018). The physicochemical properties of PAH make them a major contributor for soil and groundwater contamination through bio-magnification (Norris, 2017). Moreover, according to the Environmental Health Hazard Assessment, U.S.A., naphthalene (NAP) concentration beyond 170 ppb is not safe drinking (Bruce et al., 1998). Different orthodox and expensive techniques for environmental remediation, *viz.*, incineration, gasification, plasma-gasification have been replaced by green-technologies such as bioremediation, phytoremediation, nanoremediation, *etc.* (Thomé et al., 2018). Bioremediation is considered as the most cost-effective and eco-friendly oil spill management technique (Wilson and Jones, 1993). However, while considering the vast volume of a mobile open water system, bioremediation stumble upon several limiting factors such as the low local concentration of the effective microorganisms, loss of active microorganisms, *etc.* (Chen et al., 2017). Conversely, cell immobilization provides several advantages such as, it helps to retain high local concentration of the effective microorganisms, keep intact bacterial cell membrane stability and can be stored for future reuse (Bhardwaj et al., 2000). Overall, cell immobilization can markedly improve the stability and efficiency of the bioremediation process (Mrozik and Piotrowska-Seget, 2010; Tyagi et al., 2011). Cell immobilization using calcium alginate beads (CABs) is a convenient option where maximum cells remain viable and can tolerate high concentration of the toxicant (Lee and Heo, 2000). Moreover, calcium alginate is nontoxic to the bacterial

cell and it has low production cost which facilities easy reuse (Bhardwaj et al., 2000). Biodegradation of a toxicant (complex nutrient for bacteria) by the microbial consortium can efficiently enhance biodegradation rate (Kumari et al., 2018). This rate enhancement could be achieved by several ways such as, different biodegradation pathways of each individual bacterium (Dutta et al., 2018), a metabolic intermediates of one bacteria may act as the starting material of other bacteria (Surkatti and El-Naas, 2018), different genetic makeup (Woyke et al., 2006), synergetic effects of different microbial species, (Ghazali et al., 2004) or by synthesising different variant of catalytic enzymes. Bacterial cells in the microbial consortium can also combine their metabolic capabilities to utilize the common complex nutrient (Gilbert et al., 2003). Biodegradation of complex hydrocarbon mixture by the microbial consortium offers a combination of diverse enzymes which promotes the biodegradation processes (Wongwilaiwalin et al., 2010). However, microbial consortium immobilization for biodegradation of PAHs was not studied previously. The aim of the present study is to evaluate the naphthalene biodegradation performance by *Pseudomonas putida* strain KD10 and *Pseudomonas* sp. consortium as a free and immobilized format. Previous study showed that *Pseudomonas putida* strain KD9 cells decrease in size and shape from rod to sphere during naphthalene biodegradation and their specific growth rate was also little slower (Dutta et al., 2018). Keeping this fact in the mind, both morphological types of bacteria were applied in this present set of study. Additionally, the naphthalene 1, 2-dioxygenase (*nah*Ac) was sequenced and analyzed.

2. Materials and methods

2.1. Chemicals

Naphthalene was purchased from Sigma-Aldrich chemicals Pvt. Ltd. (USA) and all other chemicals used for media preparation were procured from HiMedia Laboratory (Mumbai, India). GC-MS and HPLC grade solvents were procured from Fisher Scientific (Mumbai, India). Sodium alginate (CAS No. 9005-38-3) of medium viscosity was purchased from Merck Pvt. Ltd. (USA).

2.2. Microorganisms, growth media, growth condition and consortium preparation

Soil samples were collected from petroleum refinery waste sites near Indian Oil (Haldia, West Bengal, India). The enrichment isolation and strain identification were carried out according to the standard protocol described previously (Dutta et al., 2017). Carbon deficient minimum medium (CSM), with a pH of 7.1, was used to cultivate the bacteria. Naphthalene was used as a sole source of carbon and energy in CSM with following compositions: 0.2 g L^{-1} $MgSO_4$, $7H_2O$; 0.08 g L^{-1} Ca $(NO_3)_2$, $4H_2O$; 0.005 g L^{-1} $FeSO_4$, $7H_2O$; 4.8 g L^{-1}, K_2HPO_4; 1.2 g L^{-1} KH_2PO_4. *Pseudomonas putida* strain KD6 (KX786159.1) and *Pseudomonas putida* strain KD9 (KX786158.1) and the newly isolated *Pseudomonas putida* strain KD10 (KX786157.1) were used to prepare the blend of *Pseudomonas* sp. consortium. The consortium was maintained in Luria-Bertani broth at 31°C with 150 rpm in order to grow the bacterial cell in its normal size and shape. Alternatively, bacterial cells were grown in CSM with naphthalene a as sole source of carbon and energy to obtain altered morphological variant.

173

174 *2.3. Gene sequence analysis*

175 *2.3.1. Detection of naphthalene 1, 2-dioxygenase and catechol 2, 3-dioxygenase*

176 The conventional polymerase chain reaction (PCR) for naphthalene 1, 2-
177 dioxygenase (*nah*Ac) and catechol 2, 3-dioxygenase (*nah*H) using specific primers
178 (Table S1) were performed. Additionally, PCR product of *nah*Ac was sequenced and
179 analyzed according to the methods described previously (Dutta et al., 2017).

180

181 *2.3.2. Clustering and phylogenetic analysis*

182 The evolutionary distance of naphthalene 1, 2-dioxygenase among different
183 bacterial species was analyzed using BLOSUM weighted matrix followed by pairwise
184 distance computation using MEGA (v7.0) (Kumar et al., 2016). The distance matrix
185 was then clustered using R (Team, 2013) to create the cladogram and heatmap. The
186 phylogenetic position of the isolated *Pseudomonas putida* strain KD10 was analyzed
187 using the previous method (Dutta et al., 2017).

188

189 *2.3.3. Molecular docking*

190 The rigid-body molecular docking was conducted using Auto Dock (v4.2.1)
191 (Morris et al., 1998). Briefly, the center grid dimensions were set to
192 20.271×61.989×87.168 with a grid spacing of 0.375 Å. The virtual screening was

193 repeated for 10 times with the unaltered docking parameters having 2.0 Å cluster
194 tolerance. Additionally, the rigid-flexible molecular docking was performed using
195 Molecular Operation Environment (Chemical Computing Group, Montreal Inc.,
196 Canada). The latter scoring function was employed to identify the most favourable
197 docked poses and to estimate the binding affinity of the protein-ligand complexes. The
198 non-covalent interactions were analyzed using the previous method (Salentin, S., et al.,
199 2015).

200

201 *2.4. Enzyme kinetic assay*

202 The enzyme kinetic parameters of the naphthalene 1, 2-dioxygenase $_{I250, V256}$ was
203 performed using the cell-free extract of the *Pseudomonas putida* strain KD10, grown in
204 250 mL of CSM with naphthalene (500 mg L^{-1}) as a sole source of carbon and energy as
205 described by previously (Dutta et al., 2017).

206

207 *2.4. Detection of solvent efflux pumps system*

208 The detection of solvent efflux pump system (*srp*ABC) in *Pseudomonas putida*
209 strain KD10 was performed using conventional polymerase chain reaction in a thermal
210 cycler (Mastercycler® nexus gradient, Eppendrof, (Germany). Standard reaction
211 mixtures were prepared using forward, reverse primers (Table S1) as described
212 previously (Dutta et al., 2018).

213

2.5. *Cell immobilization*

2.5.1. Cell immobilization in calcium alginate beads

Pseudomonas putida strain KD10 and *Pseudomonas* sp. consortium were immobilized according to the standard protocol described previously (Daâssi et al., 2014). Briefly as sodium alginate was dissolved in 0.9 wt. % NaCl (1 gm in 40 mL 0.9 wt. % NaCl) for 24 h and sterilized by autoclaving (121°C for 15 min). Two grams of bacterial cell mass was added to 8 ml of NaCl solution and again added to the sterile alginate solution. The mixture was then gently vortex for complete homogenization and extruded dropwise through a hypodermic syringe into chilled sterile $CaCl_2$ solution (Figure 2). The beads were hardened in the same solution at room temperature with gentle stirring for 1 h. Finally, the beads were washed several times with 0.9 wt. % NaCl to remove excess calcium ions and free cells. The beads have an average diameter of 0.5 mm and stored at 4°C. Sterile beads (without microorganisms) were used to monitor the abiotic loss of naphthalene. Sodium alginate of medium viscosity (≥2,000 cP) was used to prepare the calcium alginate beads (CABs).

2.5.2. Cell viability count

The viable cell enumeration in the CABs was performed by using a protocol described previously (Usha et al., 2010). In brief, CABs was washed in saline and keep submerged for 10 min (for saline soaking). Following soaking, the CABs were shaken with glass beads for 15 min and 1 g CABs were homogenized in 9 ml saline. The saline was then used for viable cell enumeration onto a nutrient agar plate. Plating was done

with this treated saline by series dilution method up to 10^{-5} dilutions on nutrient agar plates. Plating was also done for the initial CFU count. For every dilution, 10 µl of the solution was plated. Plating was done by the pour plate method. Plates were incubated at 37°C for 24 h. (Jain and Pradeep, 2005).

2.6. Scanning electron microscopic (SEM) study

Samples for SEM analysis were prepared by a protocol described elsewhere (Dutta et al., 2018). The dried samples were coated in a sputter coater (Quorum-SC7620) under vacuum with a thin gold layer right before SEM analysis using a scanning electron microscope (Zeiss, EVO 18, Germany) with an accelerating voltage of 5 kV.

2.7. Biodegradation kinetics

2.7.1. Biodegradation of naphthalene in the liquid medium

Naphthalene biodegradation study was conducted by the protocol described previously (Dutta et al., 2017). The conical flasks were incubated at 31°C with 150 rpm and uninoculated conical flask were used as control. Culture medium was collected at regular interval of 72 h for degradation and growth kinetic study. Additionally, the effect of initial concentration of naphthalene (150-2500 mg L^{-1}) was studied with different immobilized systems.

2.7.2. Chemical analysis

Naphthalene biodegradation was analyzed by using the 1260 infinity series HPLC system (Agilent, Santa Clara, CA, USA) equipped with Zorbax SB-C18 reversed-phase column (4.6 × 12.5 mm, 5 µm). The analysis of naphthalene concentrations was conducted using isocratic elution conditions with the mobile phase 80:20 (v/v) methanol: water at a flow rate of 1 ml min^{-1}. The detection was performed at 254 nm according to the protocol described in the literature (Dutta et al., 2017). Additionally, the metabolic intermediates of naphthalene biodegradation were analyzed using the GC-MS system (GC Trace GC Ultra, MS-Polarisq, Thermo Scientific India Pvt. Ltd) equipped with a capillary column (TR-WaxMS, 30 m × 0.25 mm [ID] × 0.25 µm film thickness) by the protocol described elsewhere (Dutta et al., 2017). The entire analysis was performed in electron ionization, at full scan mode. The metabolite identification was based on the mass spectra comparison using the NIST Mass Spectral library (v2.0, 2008).

2.8. Data analysis

The first-order degradation kinetics model was used to estimate the residual naphthalene in CSM using equations 1, the algorithms as expressed determine the half-life ($t_{1/2}$) values of naphthalene in CSM. The substrate inhibition kinetic parameters were calculated using equation 2.

$$C_t = C_0 \times e^{-kt} \quad [1]$$

278

$$q = q_{max} \frac{S}{K_s + S + {S^2}/{K_i}} \quad [2]$$

279

280 The effect of SCS on growth pattern was measured by calculating the difference
281 between optical densities at 600_{nm} and expressed by slight extension (Equation 4) of the
282 Gomperz's sigmoid growth fit equation (Equation 3).

283

$$y = ae^{-\exp(-k\,(x-x_c))} \quad [3]$$

284

$$\Delta X_c = X_{c2} - X_{c1} \quad [4]$$

285

286 The growth pattern change by SCS was considered as CFU shift (Equation 5). Where,
287 X_{c2} = Optical density at X_{c2} and X_{c1} = Optical density at X_{c1}.

$$CFU_{shift} = \Delta X_c \quad [5]$$

288

289 The bacterial growth kinetics were analyzed by applying the Gomperz's model using
290 Levenberg-Marquardt algorithm in Origin® 2016 (California, USA) and the degradation
291 kinetics were analyzed by using Graphpad Prism® 6.01 (San Diego, CA, USA).

292

3. Results and discussion

3.1. Isolation, identification and growth patterns of NAP degrading bacterial strain

Pseudomonas putida strain KD10 was isolated from petroleum refinery waste with its distinguished colony morphology on CSM agar plate (Figure S1a, b). The PCR product of 16S rRNA gene of the strain KD10 was sequenced. Moreover, the multiple sequence alignment followed by phylogenetic assessment suggests that the strain belongs to the *Pseudomonas putida* group and it showed 99% sequence similarity with the previously deposited sequences of *Pseudomonas putida* (Figure S2). The 16S rRNA gene sequence was deposited at NCBI (https://www.ncbi.nlm.nih.gov/) under the GenBank accession number KX786157.1.

Naphthalene biodegradation by the *Pseudomonas putida* KD10 was preliminarily confirmed by the catechol test (Figure S1C) followed by growth pattern analysis in CSM with naphthalene as a sole source of carbon and energy. Additionally, growth pattern with 0.5 gm % sucrose as a secondary carbon supplement (SCS) was compared with growth pattern of non-supplemented CSM. Gompertz's model fit (Equation 3) was used to analyze the growth curve (Table S4).

3.2. *Pseudomonas* sp. consortium, growth pattern and NAP biodegradation

The growth pattern of the *Pseudomonas* sp. consortium, as shown in Figure 1 was optimized at 31°C and pH 7.1 which reveal successful cooperation among *Pseudomonas putida* strain KD6, KD9 and KD10. Further, the growth curve model indicates a significant increase in total biomass of the *Pseudomonas* sp. consortium and they also showed a high concentration of naphthalene tolerance potential.

317 *3.3. Gene sequence and phylogenetic analysis*

318 Naphthalene 1, 2-dioxygenase (*nah*Ac), encoded by *Pseudomonas putida* strain
319 KD10 have only two point mutations at I250, and V256 which were replaced by
320 methionine and glycine respectively (Figure 3A, S6). However, additional mutations
321 were found in the same chain A at K200, A210, E264, M284 and N334 by replacing
322 glutamic acid, glycine, aspartic acid, isoleucine, respectively (Dutta et al. 2017, 2018).
323 The three dimensional structural analysis suggests that the mutations at 200, 210, 284
324 and 334 causes a little structural change in comparison to the wild type variant of
325 naphthalene 1, 2-dioxygenase (Figure 3B). Conversely, the amino acids stretch at the
326 close proximity of the active site residues exactly from 248 to 266 showed a structural
327 mismatch among all three mutant and wild type variants of naphthalene 1, 2-
328 dioxygenase (Figure 3B). The active site of an enzyme tends to evolve fast to attain its
329 maximum performance and functionality in a particular environment (James and
330 Tawfik, 2003).

331 The alteration of amino acids bases from 248 to 266 of chain A, was a common
332 feature in all three mutant variants of *nah*Ac and this particular stretch of amino acid is
333 very close to the active site residues (Figure 3C). This implies that the “248-266” amino
334 acid stretch is highly prone to mutation and it may influence on the enzymatic efficiency
335 and environmental adaptability. Thus, our study provides a new insight, which could be
336 beneficial for rational approaches of enzyme redesigning.

337 The biodegradation performance of a bacterial strain is linked with the three
338 dimensional structure of the catalytic enzyme and ligand binding posture (Singh et al.,
339 2019). Moreover, alteration of a single amino acid in the catalytic domain of the enzyme
340 caused different ligand binding postures which eventually lead to a unique

biodegradation pathways (Ferraro et al., 2006). In addition, site directed mutagenesis in the catalytic domain offers superior enzyme activity (Parales et al., 1999; Parales, 2003). The comparative analysis of binding free energy helps to comprehend the superior naphthalene biodegradation performance by the *Pseudomonas* sp. consortium, which is, in fact, the summative activity of all three mutant variants of naphthalene 1, 2-dioxygenase.

The evolutionary trace on the naphthalene 1, 2-dioxygenase among different species were studied through pairwise distance matrix analysis (Figure 4), which suggests a significant intra and inter species difference among *Sphingopyxis sp*., *Croceicoccus naphthovorans, Burkholderia multivorans, Burkholderia sp. Massilis sp. and Cycloclasticus sp*. Conversely, other *Pseudomonas* sp. particularly, *Pseudomonas benzenivorans, Pseudomonas balearica, Pseudomonas stutzeri, Pseudomonas kunmingensis, Pseudomonas frederikbergensis* have similarities in their version of naphthalene 1, 2-dioxygenase. A few other species such as *Xenophilusa zovorans, Ralsoniam annitolilytica,* and *Paraburkholderia aromaticivorans* does not show significant evolutionary distance in their version of naphthalene 1, 2-dioxygenase (Figure 4). However, a few strains of *Burkholderria multivorans* showed similarities and some other does not (Figure 4). The source of collection of these two *Burkholderria multivorans* species may be the reason for such variation (Li et al., 2007). In a study by ~~(~~Su et al., 2016~~)~~, the epigenetic impacts on the metabolic enzymes have been suggested. Moreover, the divergence of evolutionary distances of the same enzyme between different and same bacterial species indicates thrive in a particular microenvironment. However, further studies are needed to identify the underlying cause and mechanisms of such variation intra-species variation.

365

366 *3.4. Molecular docking*

367 The result depicted from the rigid body molecular docking, suggests *nah*Ac-
368 $KD10_{I250, V256}$ mutant has a little higher binding free energy than that of mutant *nah*Ac
369 encoded by KD9 but little lower than the *nah*Ac mutant variant encoded by the KD6
370 (Table 1). However, the rigid-flexible molecular docking using MOE algorithms
371 showed *nah*Ac I_{250}, G_{256} mutant variant has ΔG_{London} of -7.1 kcal mol^{-1} and $\Delta G_{GBVI/WSA}$
372 of -1.68 kcal mol^{-1}, which is little higher than other two mutant variants of *nah*Ac
373 encoded by KD6 and KD9 (Table 1). The interacting amino acid residues in the active
374 site were confined to be quite same in three mutant variants, except one variation, *i.e.*,
375 His_{208} which is located about 5.49 Å away from the bicyclic ring of naphthalene (Figure
376 3D). The altered binding free energy of the *nah*Ac-$KD10_{I250, V256}$ may be due to the fact
377 that the two altered amino acid residues reside in "248-266" and participation of His_{208}
378 as a unique interacting residue (Figure 3C). Furthermore, the non-covalent interactions
379 of the *nah*Ac-$KD10_{I250, V256}$ with naphthalene, phenanthrene and anthracene suggest that
380 Phn 352 was common residue and His 208 is involve in π- staking with a bond angle of
381 80.58° and 77.19° respectively for naphthalene and anthracene (Table S5).

382

383 *3.5. Enzyme kinetic assay*

384 Enzyme activity by cell free extract of *Pseudomonas putida* KD10 was studied
385 using Naphthalene as substrate. The cell free extract of strain KD10 degraded
386 Naphthalene, with R^2 of 0.935 indicating the experimental data are well correlated with
387 the model (Table 2). The performance constant (Kcat/ Km) was 0.142×10^3 ml^{-1} $mol.^{-1}$ s^{-1}
388 which further validate the chemical data obtained from chemical analysis (Table 1). In

389 previous study, the performance constant of *Pseudomonas putida* KD6 was little higher
390 than *Pseudomonas putida* strain KD10, suggesting the six altered amino acid residues of
391 the mutant naphthalene 1,2-dioxygenase of the KD6 may be main cause of this
392 difference (Dutta et al. 2017). The performance constant (Kcat/ Km) is the indicator of
393 the performance of an enzyme and usually the higher Kcat/Km meaning better
394 enzymatic performance (Koshland Jr DE, 2002).

395

396 *3.6. Detection of solvent efflux system*

397 The cellular microenvironment and internal homeostasis are crucial for
398 maintaining normal cellular functions and cell tends to adopt several strategies in order
399 to achieve it (Blanco et al., 2016). One such adaptation strategy is the solvent efflux
400 pump system, that control intracellular toxicity to some extent (Kusumawardhani et al.,
401 2018). The role of *srp*ABC solvent efflux pump system in the biodegradation of PAHs
402 are common in literature (Bugg et al., 2000). Besides the other cellular activities,
403 *srp*ABC also assist in gaining antimicrobial resistance (Schweizer, 2003).
404 Biodegradation studies on chlorpyrifos indicate that the intermediates formed during
405 biodegradation, act as an antimicrobial agent to other species, meaning that the
406 metabolic intermediates may have a role on inter-species competition in a particular
407 micro-environment to thrive in nutrient-limiting condition (Anwar et al., 2009), (Raes
408 and Bork, 2008). Besides, the role of *srp*ABC on biodegradation enhancement process
409 is still poorly understood. The presence of *srp*ABC in *Pseudomonas putida* strain KD10
410 (Figure S5) and the efficient naphthalene biodegradation property can be interlinked
411 (Dutta et al., 2018).

412

413 *3.7. Cell immobilization and viability count*

414 The viscosity of CABs determines its efficiency of the immobilization and its
415 performance of detoxification of environmental pollutant (Young et al., 2006).
416 Therefore, sodium alginates of medium viscosity were chosen for this study. The
417 efficiency of cell immobilization in CABs was evaluated by enumeration of viable cells
418 (Table S3). Bacteria immobilized in CABs do not significantly lose its viable biomass
419 after 21 days of incubation at 4°C.

420

421 *3.8. Naphthalene biodegradation studies*

422 *3.8.1 By free Pseudomonas putida* strain KD10

423 Biodegradation kinetics of naphthalene (500 mg L^{-1}) by the *Pseudomonas putida*
424 strain KD10 was first tested to determine its naphthalene biodegradation potential
425 (Figure 4). It was found that after 12 days of incubation at 31°C the amount of residual
426 naphthalene reduced significantly ($p<0.05$) (Figure 5). Results are also summarised at
427 Table 3 along with names of the immobilized systems. The first order degradation
428 kinetic data suggest that at the end of the incubation *Pseudomonas putida* strain KD10
429 efficiently decompose 95.22 % naphthalene in CSM as a sole source of carbon and
430 energy. The values of degradation rate constant (k) and half-life ($t_{1/2}$) were 0.2193 and
431 3.1 days with R^2 of 0.981. In the previous study, 99.1 % of initial naphthalene was
432 removed within 96 h by strain *Bacillus fusiformis* (BFN). However, the initial
433 concentration was very low (50 mg L^{-1} of initial naphthalene) (Lin et al., 2010).

434 After confirmation of naphthalene biodegradation potential of *Pseudomonas*
435 *putida* strain KD10, the stain was allowed to grow in association with other two strains
436 of *Pseudomonas putida*, namely *Pseudomonas putida* strain KD6 and *Pseudomonas*

437 *putida* strain KD9 (Dutta et al., 2017; Dutta et al., 2018). These two strains were
438 selected to develop the blend of *Pseudomonas* sp. consortium, because they were
439 collected from different isolation points, they encode different variant of *nah*Ac and
440 they have common optimized growth parameters (temperature 31°C and pH 7.1) (Dutta
441 et al., 2017 & Dutta et al., 2018). Further, *Pseudomonas putida* strain KD6 encodes a
442 six point mutant *nah*Ac with the capability to co-degrade high concentration of
443 naphthalene, phenanthrene (PHN) and pyrene (PYR), (500 mg L^{-1} each). Moreover, the
444 stain KD9 encodes a four point mutant variant of *nah*Ac with rhamnolipid production
445 capabilities (Dutta et al. 2018).

446 In the previous study, $t_{1/2}$ of naphthalene co-biodegradation with phenanthrene
447 and pyrene by *Pseudomonas putida* strain KD6 was 4.1 days, which was significantly
448 reduced to 2.2 days when bacterial cells were allowed to grow as *Pseudomonas* sp.
449 consortium with only naphthalene (Table 3). Further, this value was found as 2.7 days
450 for *Pseudomonas putida* KD9, suggesting *Pseudomonas putida* strain KD6 might face
451 some sort of substrate inhibition by the co-presence PHN and PYR in the system (Jiang
452 et al., 2018) and the cooperative nature of the *Pseudomonas* sp. consortium helps to
453 enhance the naphthalene bio-utilization. The microbial consortium works several ways,
454 *viz.*, by the division of labor, cross-feeding, *etc.* (Smid and Lacroix, 2013). Moreover, a
455 successful consortium could also overcome shortcomings of single bacteria (Bhatia et
456 al., 2018). However, it is a fact that, bacteria select PAH among mixed PAHs based on
457 their structural simplicity first (Dutta et al., 2017) and the velocity could be optimized
458 by reducing the initial concentration of the PAHs gradually according to the structural
459 simplicity (Jiang et al., 2018).
460

461 *3.8.2. By immobilized Pseudomonas* sp. *consortium*

462 The biodegradation kinetic of naphthalene by individual *Pseudomonas putida*
463 strain KD6, KD9, KD10 and *Pseudomonas* sp. consortium immobilized in CABs,
464 depicted further enhancement of overall naphthalene bio-utilization (Table 3). Cell
465 immobilization using hydrogel, such as CAB found to be advantageous rather than free
466 cells (Hameed and Ismail, 2018).

467 This phenomenon may be attributable due to the increased level of tightness of
468 the cross-linked polymers of the calcium alginate beads that render bacteria adequate
469 amount of protection from harsh environment (Chen et al., 2013). However, the free
470 bacterial cell lacks the capabilities to degrade a high initial concentration of the toxicant
471 because they followed the conventional growth phases (Marrot et al., 2006). In addition,
472 exposure of free bacterial cells to the high initial concentration of toxicants may
473 challenge them to experience shock-concentration (Zhao et al., 2006). Conversely, cells
474 immobilized in calcium alginate beads can tolerate high concentration of the toxicant
475 and decrease the lag phase duration (Kao et al., 2014). Moreover, the diffusion
476 limitation natures of the CABs matrix provide a high local concentration of the cell
477 population (Bezbaruah et al., 2009). Furthermore, CABs provides remarkable stability
478 and reusable features that effectively reduces the production cost (Daâssi et al., 2014).

479 Biodegradation of naphthalene by immobilized *Pseudomonas* sp. consortium
480 significantly elevated the overall naphthalene bio-utilization efficiency with $t_{1/2}$ and R^2
481 values of 2 days and 0.998 respectively, suggesting experimental data are well
482 correlated to the model (Table 3). The individual cell population also displayed
483 improved biodegradation efficiency. However, the biodegradation efficiency was
484 maximum by *Pseudomonas putida* strain KD6, which showed a marked reduction of $t_{1/2}$

485 from 4.1 to 3.0 days (Table 3). It promptly suggests that CABs facilitate KD6 optimized
486 naphthalene bio-utilization, that might be masked-up by the co-presence of NAP, PHN,
487 PYR (Jiang et al., 2018). However, further studies are required to investigate
488 behavioural patterns of a consortium with mixed PAH.
489
490 Bacterial cell grown on CSM with naphthalene as a sole source of carbon and
491 energy showed a delayed growth rate and their total biomass was also low (Figure 1).
492 Nevertheless, growing cells on CSM prior to immobilization in CABs provide them
493 essential adaptation to the toxicant and mature them for such stress condition (Table 3).
494 Immobilized cell system was useful for bioremediation of a toxicant after prior
495 adaptation to the surrounding environment (Partovinia and Rasekh, 2018). However,
496 growing cells in Luria-Bertani broth does not adapt cell adequately, and their
497 naphthalene removal performance was very poor (Figure S3). The inoculum was
498 normalized (OD_{600nm} = 0.002) for each *Pseudomonas putida* strain in order to prepare
499 the *Pseudomonas* sp. consortium. In aqueous medium, the immobilized bacterial cell
500 mainly on the surface was exposed to naphthalene and primarily involved in the
501 naphthalene bio-utilization process. However, due to the micro-porous feature of the
502 calcium alginate beads, microbial cells immobilized other than surface are also
503 participates in the bio-utilization and bio-sorption process of naphthalene. Further, with
504 time due to the mechanical force generated by shaking, a few microbial cells may
505 release from the calcium alginate beads. However, to fuel up the cell, it is necessary to
506 uptake naphthalene for bio-utilization through step by step intracellular enzymatic
507 reactions (Lin et al., 2014).
508

509

510 *3.8.3. Effect of initial naphthalene concentration on biodegradation kinetics*

511 The effect of different initial concentration of naphthalene (150 – 2500 mg L^{-1})
512 on degradation kinetics was evaluated with immobilized KD6, KD9, and KD10 as
513 individual and as a consortium (Table S2). The results suggest cell immobilization in
514 CABs facilitates bacteria to cope with a high initial concentration of NAP (Table S2).
515 The substrate inhibition kinetic parameters, *viz.*, the maximum specific degradation rate
516 (q_{max}), and inhibition constant (k_i) were highest for immobilized *Pseudomonas* sp.
517 consortium and these values were 0.707 h^{-1} and 1475 mg L^{-1} respectively (Table S2).
518 However, we did not find any significant change on half saturation constant (k_s),
519 suggesting the reaction does not depend on its initial concentration and the
520 biodegradation process follows pseudo-first order reaction kinetics. In previous study,
521 free *Pseudomonas putida* KD9 in CSM was capable to tolerate relatively low initial
522 concentration of naphthalene with k_i value of 1107 mg L^{-1} and addition of sucrose as
523 SCS provides quite similar potential of naphthalene tolerance (k_i of 1429 mg L^{-1}) with
524 that of immobilized *Pseudomonas* sp. consortium (Dutta et al., 2018). However, sucrose
525 (0.5 gm. %) in the mobile open water system would not be beneficial for bacteria to
526 overcome the high shock concentration of the toxicant, again suggesting cell
527 immobilization and development of effective microbial consortium as systematic
528 optimization of biodegradation process.

529 *3.9. Detection of metabolic end products*

530 The metabolic pathway of naphthalene biodegradation that might be followed by
531 *Pseudomonas putida* strain KD10 was elucidated through GCMS analysis of the

532 metabolites (Figure S4). In the previous study, the major metabolites ware restricted to
533 be salicylaldehyde, catechol, D-gluconic acid and pyruvic acid (Dutta et al., 2018).
534 However, in the present study, we have detected salicylic acid as an additional
535 metabolite (Table 4). Catechol step into the TCA cycle by two possible pathway one is
536 ortho-cleavage and another is meta-cleavage pathway. The meta-cleavage pathway is
537 led by catechol-2, 3-dioxygenase (*nah*H), and presence of *nah*H (Figure S5) suggesting
538 in *Pseudomonas putida* stain KD10 opt the meta-cleavage pathway. Furthermore, we
539 assume that D-gluconic acid enters in the bio-conversion of naphthalene, possibly from
540 glucose as a precursor (Figure 6) and it is finally converted to pyruvate via aldolase. D-
541 gluconic acid implies impotence between bacteria-plant mutualistic association e.g.,
542 induction of phosphate solubilization processes (Rodriguez et al., 2004) which can
543 inhibit fungal growth (Kaur et al., 2006). The metabolic intermediates *viz.*, salicylic
544 acid, catechol has plant-growth promoting activity (Lee et al., 2010) e.g., the antioxidant
545 property of the catechol help and promotes seed germination (Schweigert et al., 2001).
546 The presence of d-gluconic acid as a major metabolite and its subsequent entry in TCA
547 cycle from glucose precursor, suggest that KD10 may able to sequestered catechol upon
548 needs to promote the plants' growth (Figure 6).

549

550 *4. Conclusion*

551

552 Naphthalene biodegradation by free and immobilized *Pseudomonas putida*
553 strain KD10 and *Pseudomonas* sp. consortium were studied. HPLC analysis showed
554 80.1% of initial naphthalene (500 mg L^{-1}) was utilized by immobilized *Pseudomonas*

555 sp. consortium after 72 h of incubation. Further, initial naphthalene tolerance by
556 immobilized *Pseudomonas* sp. consortium was highest (1475 mg L^{-1}) with maximum
557 specific degradation of 0.707 h^{-1}. The gene sequence analysis of the naphthalene 1, 2-
558 dioxygenase suggests a significant evolutionary distance among different microbial
559 species and in few cases, intra-species variation was observed. A common mutation
560 prone amino acid stretch inside Chain A of all three natural mutant variants of
561 naphthalene 1, 2-dioxygenase were found at close proximity of the active site. Further,
562 the rigid-flexible molecular docking showed better binging free energy of the mutant
563 variant encoded by *Pseudomonas putida* strain KD10 than that of wild-type variant of
564 naphthalene 1,2-dioxygenase. This common mutation prone amino acid stretch could
565 aid the rational approaches of enzyme redesigning. Overall, this study summarises the
566 application of bacterial cell immobilization in calcium alginate beads and development
567 of the microbial consortium together for enhanced naphthalene biodegradation.
568 However, further studies are required for the systematic optimization of naphthalene
569 biodegradation in a real environment.

570

571 *Authors Contributions*

572 KD and CG conceive the main hypothesis. KD design, performed all
573 experiments, and wrote the manuscript. SS, IK, SB, DJ assisted KD in some
574 experiments. MK, TM, PR, KCG performed the statistical analysis and wrote the
575 manuscript. CG critically proofread and wrote the manuscript. All authors read the
576 manuscript.

577

Funding

University Grant Commission (UGC) Govt. of India, New Delhi, India (Grant No. VU/Innovative/Sc/17/2015).

Acknowledgement

University Grant Commission (UGC) Govt. of India, New Delhi, India (Grant No. VU/Innovative/Sc/17/2015) is acknowledged by C.G. K.D. acknowledges Council of Scientific and Industrial Research (CSIR), Govt. of India, New Delhi, India for Senior Research Fellowship (SRF) sanction letter no. 09/599 (0082) 2K19 EMR-Z dated: 29/03/2019.

Conflict of Interest

The authors declare that they have no conflict of interests.

References

Anwar, S., Liaquat, F., Khan, Q.M., Khalid, Z.M., and Iqbal, S. (2009). Biodegradation of chlorpyrifos and its hydrolysis product 3, 5, 6-trichloro-2-pyridinol by Bacillus pumilus strain C2A1. *Journal of Hazardous Materials* 168(1)**,** 400-405.

Bernstein, H.C., Paulson, S.D., and Carlson, R.P. (2012). Synthetic Escherichia coli consortia engineered for syntrophy demonstrate enhanced biomass productivity. *Journal of biotechnology* 157(1)**,** 159-166.

Bezbaruah, A.N., Krajangpan, S., Chisholm, B.J., Khan, E., and Bermudez, J.J.E. (2009). Entrapment of iron nanoparticles in calcium alginate beads for groundwater remediation applications. *Journal of Hazardous Materials* 166(2-3)**,** 1339-1343.

603 Bhardwaj, T.R., Kanwar, M., Lal, R., and Gupta, A. (2000). Natural gums and modified
604 natural gums as sustained-release carriers. *Drug development and industrial*
605 *pharmacy* 26(10)**,** 1025-1038.

606 Bhatia, S.K., Bhatia, R.K., Choi, Y.-K., Kan, E., Kim, Y.-G., and Yang, Y.-H. (2018).
607 Biotechnological potential of microbial consortia and future perspectives.
608 *Critical reviews in biotechnology* 38(8)**,** 1209-1229.

609 Blanco, P., Hernando-Amado, S., Reales-Calderon, J., Corona, F., Lira, F., Alcalde-
610 Rico, M., et al. (2016). Bacterial multidrug efflux pumps: much more than
611 antibiotic resistance determinants. *Microorganisms* 4(1)**,** 14.

612 Bruce, R.M., Haber, L., and McClure, P. (1998). *Toxicological Review of Naphthalene*
613 *(CAS No. 91-20-3): In Support of Summary Information on the Integrated Risk*
614 *Information System (IRIS)*. US Environmental Protection Agency, National
615 Center for Environmental Assessment.

616 Bugg, T., Foght, J.M., Pickard, M.A., and Gray, M.R. (2000). Uptake and active efflux
617 of polycyclic aromatic hydrocarbons by Pseudomonas fluorescens LP6a.
618 *Applied and environmental microbiology* 66(12)**,** 5387-5392.

619 Chen, D.-Z., Fang, J.-Y., Shao, Q., Ye, J.-X., Ouyang, D.-J., and Chen, J.-M. (2013).
620 Biodegradation of tetrahydrofuran by Pseudomonas oleovorans DT4
621 immobilized in calcium alginate beads impregnated with activated carbon fiber:
622 mass transfer effect and continuous treatment. *Bioresource technology* 139**,** 87-
623 93.

624 Chen, Q., Li, J., Liu, M., Sun, H., and Bao, M. (2017). Study on the biodegradation of
625 crude oil by free and immobilized bacterial consortium in marine environment.
626 *PloS one* 12(3)**,** e0174445.

627 Daâssi, D., Rodríguez-Couto, S., Nasri, M., and Mechichi, T. (2014). Biodegradation of
628 textile dyes by immobilized laccase from Coriolopsis gallica into Ca-alginate
629 beads. *International Biodeterioration & Biodegradation* 90**,** 71-78.

630 Dutta, K., Shityakov, S., Das, P.P., and Ghosh, C. (2017). Enhanced biodegradation of
631 mixed PAHs by mutated naphthalene 1,2-dioxygenase encoded by Pseudomonas
632 putida strain KD6 isolated from petroleum refinery waste. *3 Biotech* 7(6)**,** 365.
633 doi: 10.1007/s13205-017-0940-1.

634 Dutta, K., Shityakov, S., Khalifa, I., Mal, A., Moulik, S.P., Panda, A.K., et al. (2018).
635 Effects of secondary carbon supplement on biofilm-mediated biodegradation of
636 naphthalene by mutated naphthalene 1, 2-dioxygenase encoded by Pseudomonas
637 putida strain KD9. *Journal of Hazardous Materials* 357**,** 187-197. doi:
638 https://doi.org/10.1016/j.jhazmat.2018.05.024.

639 Ferraro, D.J., Okerlund, A.L., Mowers, J.C., and Ramaswamy, S. (2006). Structural
640 basis for regioselectivity and stereoselectivity of product formation by
641 naphthalene 1, 2-dioxygenase. *Journal of Bacteriology* 188(19)**,** 6986-6994.

642 Ghazali, F.M., Rahman, R.N.Z.A., Salleh, A.B., and Basri, M. (2004). Biodegradation
643 of hydrocarbons in soil by microbial consortium. *International Biodeterioration*
644 *& Biodegradation* 54(1)**,** 61-67.

645 Gilbert, E., Walker, A., and Keasling, J. (2003). A constructed microbial consortium for
646 biodegradation of the organophosphorus insecticide parathion. *Applied*
647 *microbiology and biotechnology* 61(1)**,** 77-81.

648 Hameed, B.B., and Ismail, Z.Z. (2018). Decolorization, biodegradation and
649 detoxification of reactive red azo dye using non-adapted immobilized mixed
650 cells. *Biochemical Engineering Journal* 137**,** 71-77.

651 James, L.C., and Tawfik, D.S. (2003). Conformational diversity and protein evolution–a
652 60-year-old hypothesis revisited. *Trends in biochemical sciences* 28(7)**,** 361-368.

653 Jiang, Y., Zhang, Z., and Zhang, X. (2018). Co-biodegradation of pyrene and other
654 PAHs by the bacterium Acinetobacter johnsonii. *Ecotoxicology and*
655 *environmental safety* 163**,** 465-470.

656 Kao, P.-M., Hsu, B.-M., Huang, K.-H., Tao, C.-W., Chang, C.-M., and Ji, W.-T. (2014).
657 Biohydrogen production by immobilized co-culture of Clostridium butyricum
658 and Rhodopseudomonas palustris. *Energy Procedia* 61**,** 834-837.

659 Kaur, R., Macleod, J., Foley, W., and Nayudu, M. (2006). Gluconic acid: An antifungal
660 agent produced by Pseudomonas species in biological control of take-all.
661 *Phytochemistry* 67(6)**,** 595-604.

662 Koshland Jr DE. (2002). The application and usefulness of the ratio kcat/KM.
663 *Bioorganic chemistry*. 30(3), 211-3. doi: https://doi.org/10.1006/bioo.2002.1246

664 Kumar, S., Stecher, G., and Tamura, K. (2016). MEGA7: molecular evolutionary
665 genetics analysis version 7.0 for bigger datasets. *Molecular biology and*
666 *evolution* 33(7)**,** 1870-1874.

667 Kumari, S., Regar, R.K., and Manickam, N. (2018). Improved polycyclic aromatic
668 hydrocarbon degradation in a crude oil by individual and a consortium of
669 bacteria. *Bioresource technology* 254**,** 174-179.

670 Kusumawardhani, H., Hosseini, R., and de Winde, J.H. (2018). Solvent tolerance in
671 bacteria: fulfilling the promise of the Biotech Era? *Trends in biotechnology*.

672 Lee, K.-Y., and Heo, T.-R. (2000). Survival of Bifidobacterium longumImmobilized in
673 calcium alginate beads in simulated gastric juices and bile salt solution. *Applied*
674 *and environmental microbiology* 66(2)**,** 869-873.

675 Lee, S., Kim, S.G., and Park, C.M. (2010). Salicylic acid promotes seed germination
676 under high salinity by modulating antioxidant activity in Arabidopsis. *New*
677 *Phytologist* 188(2)**,** 626-637.

678 Li, X., He, J., and Li, S. (2007). Isolation of a chlorpyrifos-degrading bacterium,
679 Sphingomonas sp. strain Dsp-2, and cloning of the mpd gene. *Research in*
680 *Microbiology* 158(2)**,** 143-149.

681 Lin, C., Gan, L., and Chen, Z.-L. (2010). Biodegradation of naphthalene by strain
682 Bacillus fusiformis (BFN). *Journal of Hazardous Materials* 182(1-3)**,** 771-777.

683 Lin, C., Gan, L., Chen, Z., Megharaj, M., and Naidu, R. (2014). Biodegradation of
684 naphthalene using a functional biomaterial based on immobilized Bacillus
685 fusiformis (BFN). *Biochemical Engineering Journal* 90**,** 1-7.

686 Marrot, B., Barrios-Martinez, A., Moulin, P., and Roche, N. (2006). Biodegradation of
687 high phenol concentration by activated sludge in an immersed membrane
688 bioreactor. *Biochemical Engineering Journal* 30(2)**,** 174-183.

689 Morris, G.M., Goodsell, D.S., Halliday, R.S., Huey, R., Hart, W.E., Belew, R.K., et al.
690 (1998). Automated docking using a Lamarckian genetic algorithm and an
691 empirical binding free energy function. *Journal of computational chemistry*
692 19(14)**,** 1639-1662.

693 Mrozik, A., and Piotrowska-Seget, Z. (2010). Bioaugmentation as a strategy for
694 cleaning up of soils contaminated with aromatic compounds. *Microbiological*
695 *research* 165(5)**,** 363-375.

696 Norris, R.D. (2017). "In-situ bioremediation of soils and ground water contaminated
697 with petroleum hydrocarbons," in *Handbook of Bioremediation (1993)*. CRC
698 Press), 17-38.

699 Parales, R.E. (2003). The role of active-site residues in naphthalene dioxygenase.
700 *Journal of Industrial Microbiology and Biotechnology* 30(5)**,** 271-278.

701 Parales, R.E., Parales, J.V., and Gibson, D.T. (1999). Aspartate 205 in the catalytic
702 domain of naphthalene dioxygenase is essential for activity. *Journal of*
703 *Bacteriology* 181(6)**,** 1831-1837.

704 Partovinia, A., and Rasekh, B. (2018). Review of the immobilized microbial cell
705 systems for bioremediation of petroleum hydrocarbons polluted environments.
706 *Critical Reviews in Environmental Science and Technology* 48(1)**,** 1-38.

707 Raes, J., and Bork, P. (2008). Molecular eco-systems biology: towards an understanding
708 of community function. *Nature Reviews Microbiology* 6(9)**,** 693.

709 Rodriguez, H., Gonzalez, T., Goire, I., and Bashan, Y. (2004). Gluconic acid production
710 and phosphate solubilization by the plant growth-promoting bacterium
711 Azospirillum spp. *Naturwissenschaften* 91(11)**,** 552-555.

712 Schweigert, N., Zehnder, A.J., and Eggen, R.I. (2001). Chemical properties of catechols
713 and their molecular modes of toxic action in cells, from microorganisms to
714 mammals: minireview. *Environmental microbiology* 3(2)**,** 81-91.

715 Schweizer, H.P. (2003). Efflux as a mechanism of resistance to antimicrobials in
716 Pseudomonas aeruginosa and related bacteria: unanswered questions. *Genet Mol*
717 *Res* 2(1)**,** 48-62.

718 Singh, N.S., Sharma, R., and Singh, D.K. (2019). Identification of enzyme (s) capable
719 of degrading endosulfan and endosulfan sulfate using in silico techniques.
720 *Enzyme and Microbial Technology* 124**,** 32-40.

721 Smid, E.J., and Lacroix, C. (2013). Microbe–microbe interactions in mixed culture food
722 fermentations. *Current opinion in biotechnology* 24(2)**,** 148-154.

723 Su, X., Wellen, K.E., and Rabinowitz, J.D. (2016). Metabolic control of methylation
724 and acetylation. *Current opinion in chemical biology* 30**,** 52-60.

725 Surkatti, R., and El-Naas, M. (2018). Competitive interference during the
726 biodegradation of cresols. *International Journal of Environmental Science and*
727 *Technology* 15(2)**,** 301-308.

728 Team, R.C. (2013). R: A language and environment for statistical computing.

729 Thomé, A., Reginatto, C., Vanzetto, G., and Braun, A.B. (Year). "Remediation
730 Technologies Applied in Polluted Soils: New Perspectives in This Field", in:
731 *The International Congress on Environmental Geotechnics*: Springer), 186-203.

732 Tyagi, M., da Fonseca, M.M.R., and de Carvalho, C.C. (2011). Bioaugmentation and
733 biostimulation strategies to improve the effectiveness of bioremediation
734 processes. *Biodegradation* 22(2)**,** 231-241.

735 Usha, M., Sanjay, M., Gaddad, S., and Shivannavar, C. (2010). Degradation of h-acid
736 by free and immobilized cells of Alcaligenes latus. *Brazilian Journal of*
737 *Microbiology* 41(4)**,** 931-945.

738 Wang, L., Zhang, S., Wang, L., Zhang, W., Shi, X., Lu, X., et al. (2018). Concentration
739 and risk evaluation of polycyclic aromatic hydrocarbons in urban soil in the
740 typical semi-arid city of Xi'an in Northwest China. *International journal of*
741 *environmental research and public health* 15(4)**,** 607.

742 Wilson, S.C., and Jones, K.C. (1993). Bioremediation of soil contaminated with
743 polynuclear aromatic hydrocarbons (PAHs): a review. *Environmental pollution*
744 81(3)**,** 229-249.

Wongwilaiwalin, S., Rattanachomsri, U., Laothanachareon, T., Eurwilaichitr, L., Igarashi, Y., and Champreda, V. (2010). Analysis of a thermophilic lignocellulose degrading microbial consortium and multi-species lignocellulolytic enzyme system. *Enzyme and Microbial Technology* 47(6)**,** 283-290.

Woyke, T., Teeling, H., Ivanova, N.N., Huntemann, M., Richter, M., Gloeckner, F.O., et al. (2006). Symbiosis insights through metagenomic analysis of a microbial consortium. *Nature* 443(7114)**,** 950.

Young, C.C., Rekha, P., Lai, W.A., and Arun, A. (2006). Encapsulation of plant growth-promoting bacteria in alginate beads enriched with humic acid. *Biotechnology and bioengineering* 95(1)**,** 76-83.

Zhao, X., Wang, Y., Ye, Z., Borthwick, A.G., and Ni, J. (2006). Oil field wastewater treatment in biological aerated filter by immobilized microorganisms. *Process Biochemistry* 41(7)**,** 1475-1483.

774 *Figure legends*

775 **Figure 1.** Growth kinetic model of *Pseudomonas putida* and *Pseudomonas* sp.
776 consortium during naphthalene biodegradation. **A.** Gompertz's growth kinetic
777 model fit of the biodegradation of naphthalene by *Pseudomonas putida* strain
778 KD10 and by the *Pseudomonas* sp. consortium. **B.** Effect of 0.5 gm. % sucrose
779 supplementation on growth pattern of *Pseudomonas putida* strain KD10 and
780 *Pseudomonas* sp. consortium.

781 **Figure 2.** Cell immobilization in calcium alginate beads (CABs) with different
782 cell morphology of the *Pseudomonas putida* strain KD10.
783

784 **Figure 3**. Sequence and structure analysis of the naphthalene 1, 2-dioxygenase
785 (*nah*Ac) encoded by *Pseudomonas putida*. **A**. The amino acid sequence of wild
786 type and three mutant variants of the naphthalene 1, 2-dioxygenase (*nah*Ac).
787 Mutated residues are highlighted in blue and the common mutation prone amino
788 acid stretch is highlighted with red box. **B.** Structural mismatches among mutant
789 variants and wild type naphthalene 1, 2-dioxygenase. Each mutated residues and
790 its subsequent neighbour residues of all the mutant variant of naphthalene 1, 2-
791 dioxygenase is overlaid with cartoon representation. The highlighted red circle
792 indicates local mismatch among the mutant variant of naphthalene 1, 2-
793 dioxygenase **C.** Different ligand binding posture of the naphthalene 1, 2-
794 dioxygenase encoded by *Pseudomonas putida* strain KD10. Naphthalene (red),
795 phenanthrene (cyan) and anthracene (green) binding postures with major
796 interacting amino acid residues (left). Two-dimensional presentation of the
797 interacting residues of *nah*Ac$_{I250, V256}$ (right). **D.** Docking pose of naphthalene 1,
798 2-dioxygenase (Chain A) encoded by *Pseudomonas putida* strain KD10. The
799 four major naphthalene interacting residues and their molecular distance are
800 labelled in black.

801

802

Figure 4. Distance matrix and cladogram of the naphthalene 1, 2-dioxygenase. The evolutionary distance of the naphthalene 1, 2-dioxygenase I_{250}, V_{255} variant encoded by *Pseudomonas putida* strain KD10 other variants by different microbial species is scaled by colour index (upper-left side).

Figure 5. Naphthalene degradation kinetics of *Pseudomonas putida* strain KD10 and *Pseudomonas* sp. consortium free and cell immobilized in calcium alginate beads.

Figure 6. Proposed pathway of naphthalene biodegradation by *Pseudomonas putida* strain KD10. Naphthalene (I), salicylic acid (II), salicylaldehyde (III), catechol (IV), pyruvate (V), glucose (VI), d-gluconic acid (VII). The grey arrow indicates alternative pathway via d-gluconic acid.

Table captions

Table 1. Summary of rigid-flexible molecular docking for the analysed mutant naphthalene 1, 2-dioxygenase encoded by different *Pseudomonas putida* strains.

Table 2. Apparent enzyme kinetic parameters of naphthalene 1, 2-dioxygenase $_{I250, V256}$ encoded by *Pseudomonas putida* strain KD10.

Table 3. Parameters of first-order biodegradation kinetics of naphthalene by different free and immobilized *Pseudomonas putida* strains.

Table 4. Major metabolite detected by GCMS analysis during naphthalene biodegradation by *Pseudomonas putida* KD10.

Supplementary section

Table S1. Nucleotide sequences used as primer in polymerase chain reactions

Table S2. Parameters of substrate inhibition kinetic model of naphthalene biodegradation by different *Pseudomonas putida* strains immobilized in calcium alginate beads.

Table S3. Enumeration of viable cell in calcium alginate beads.

Table S4. Gompertz's growth curve model fit of *Pseudomonas putida* strain KD10 and *Pseudomonas* sp. consortium.

Table S5. Major amino acid residues of mutant variant of naphthalene 1, 2-dioxygenase $_{I250, V256}$ involve in hydrophobic interaction with different ligands.

Figure S1. Colony morphology and catechol confirmatory test. **A.** Colony morphology of *Pseudomonas putida* strain KD10 after 24 h of incubation. **B.** Colony morphology of *Pseudomonas putida* strain KD10 after one week of incubation.

Figure S2. Molecular phylogenetic analysis of *Pseudomonas putida* strain KD10.

Figure S3. Effect of cell adaptation on naphthalene biodegradation.

Figure S4. Mass spectra of the major metabolites detected during biodegradation of naphthalene in CSM as sole source of carbon and energy by *Pseudomonas putida* KD10.

Figure S5. Agarose gel electrophoresis of PCR products of catechol 2, 3-dioxygenase (*nah*H) gene and solvent efflux pump (*srp*ABC) system.
A. Catechol 2, 3-dioxygenase (*nah*H). Lane 1 and 2 *nah*H pcr product of *Pseudomonas putida* strain KD9 and *Pseudomonas putida* strain KD10. **B.** Solvent efflux pump (*srp*ABC) system. Lane 1: *Pseudomonas aeruginoasa* ATCC 9027, Lane 2: *Pseudomonas putida* strain KD10. Lane M: 100bp DNA ladder (HiMedia, India), Lane 3: Negative control.

Figure S6. Nucleotide sequence chromatogram of the mutant naphthalene 1, 2-dioxygenase (*nah*Ac), (chain-A) encoded by *Pseudomonas putida* strain KD10.

874
875
876
877

Table 1. Summary of rigid-flexible molecular docking of naphthalene and different mutant version of naphthalene 1, 2-dioxygenase encoded by different *Pseudomonas putida* strains

ΔG*			LB[4]	IC[5]	IME[6]	VDW[7]	RMSD[c]	RMSD[r]	References
BE[1]	London[2]	GBVI/ WSA[3]							
-5.92[a]	-7.18	-4.61	-0.59	46.14	-5.92	-5.91	0.00	77.29	Dutta et al., 2017
-5.41[b]	-7.13	-4.02	-0.54	109.07	-5.41	-5.4	0.00	96.32	Dutta et al., 2019
-5.83[c]	-7.10	-1.68	-0.58	53.13	-5.83	-5.84	0.00	96.08	This study

*PubChem ligand CID 931 = Naphthalene, BE[1] = Binding free energy, [2]London free energy, [3]Generalized born volume integral/weighted surface areas, LB[4] = ligand binding, IC[5] = inhibition constant, IME[6] = Intermolecular energy, VDW[7] = Vdw hb desolv energy, RMSD[c] = Cluster RMSD, RMSD[r] = Reference RMSD. Energy unit = kcal mol^{-1}. Inhibition constant unit = µM.at 298.15 K. Naphthalene 1, 2-dioxygenase encoded by (a) *Pseudomonas putida* strain KD6, (b) *Pseudomonas putida* strain KD9 and (c) *Pseudomonas putida* strain KD10.

878
879
880
881
882
883
884
885
886
887
888
889
890
891
892
893
894
895
896
897
898

Table 2. Apparent enzyme kinetic parameters of naphthalene 1, 2-dioxygenase $_{I250, V256}$ encoded by *Pseudomonas putida* strain KD10

Substrate	Kinetic parameters*				
	Km (μmol mL^{-1})	Vmax (μmol min^{-1})	Kcat (s^{-1})	Kcat/Km (mL^{-1} mol^{-1} s^{-1})	R^{2**}
Naphthalene	0.867	2.474	123.72	0.142×10^{3}	0.938

*The kinetic constants were determined at 30°C and pH 7.5 using 0.5-10µM ml^{-1} substrate concentration (each) by Lineweaver–Burk plot.
** Non-liner regression between initial substrate concentration 1/[S] and degradation rate constant 1/V yielded regression equation and regression coefficient (R^2)

928
929
930
931
932
933
934
935
936
937
938
939
940

Table 3. Parameters of first-order biodegradation kinetics of naphthalene by different free and immobilized *Pseudomonas putida* strains

CSM	Cells immobilized in CABs			free cells			
	k ($Days^{-1}$)	$t_{½}$ ($Days^{-1}$)	R^2	k ($Days^{-1}$)	$t_{½}$ ($Days^{-1}$)	R^2	References
A	0.228±0.005	3.0±0.077	0.99	0.167±0.012	4.1±0.307	0.98	Dutta et al., 2017
B	0.312±0.014	2.2±0.102	0.93	0.252±0.019	2.7±0.193	0.99	Dutta et al., 2018
C	0.284±0.017	2.4±0.143	0.97	0.219±0.009	3.1±0.137	0.92	This study
D	0.341±0.294	2.0±0.186	0.99	0.309±0.020	2.2±0.141	0.98	This study

[#]Initial naphthalene concentration = 500 mg L^{-1}
A. *Pseudomonas putida* strain KD6, B. *Pseudomonas putida* strain KD9, C. *Pseudomonas putida* strain KD10. D. *Pseudomonas* sp. consortium.
Each figure of the table represents the mean of three replicates.

941
942
943
944
945
946
947
948
949
950
951

Table 4. Major metabolites detected by GCMS analysis during naphthalene biodegradation by *Pseudomonas putida* KD10

Metabolite	R_t (min)	Major ion peaks (m/z)	Suggested structure
I	9.41	64.19, 92.17, 120.21, 138.22, 169.14, 191.18, 211.10	Salicylic acid
II	15.27	65.17, 74.41, 104.73, 121.10, 122.57, 142.21, 174.80, 201.22, 249.31	Salicylaldehyde
III	18.71	64.29, 81.35, 91.61, 110.47, 131.47, 149.71	Catechol
IV	31.89	61.21, 73.44, 76.24, 104.18, 117.41, 133.27, 177.23	D-gluconic acid
V	10.47	43.21, 61.27, 71.37	Pyruvic acid

R_t = Retention time

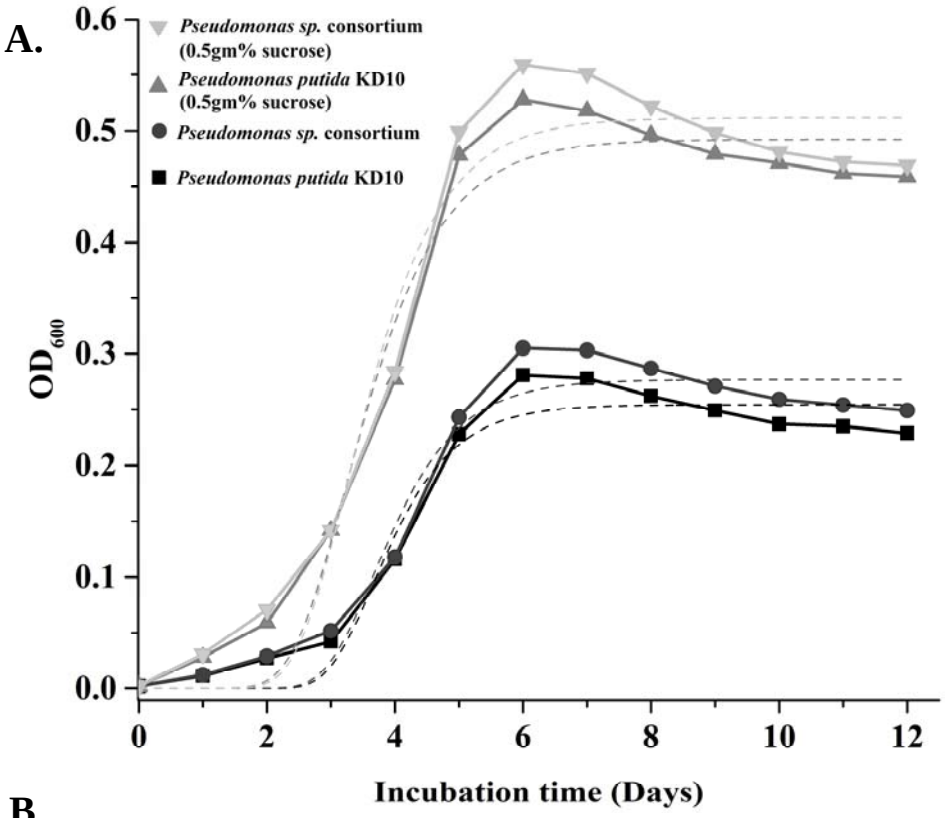

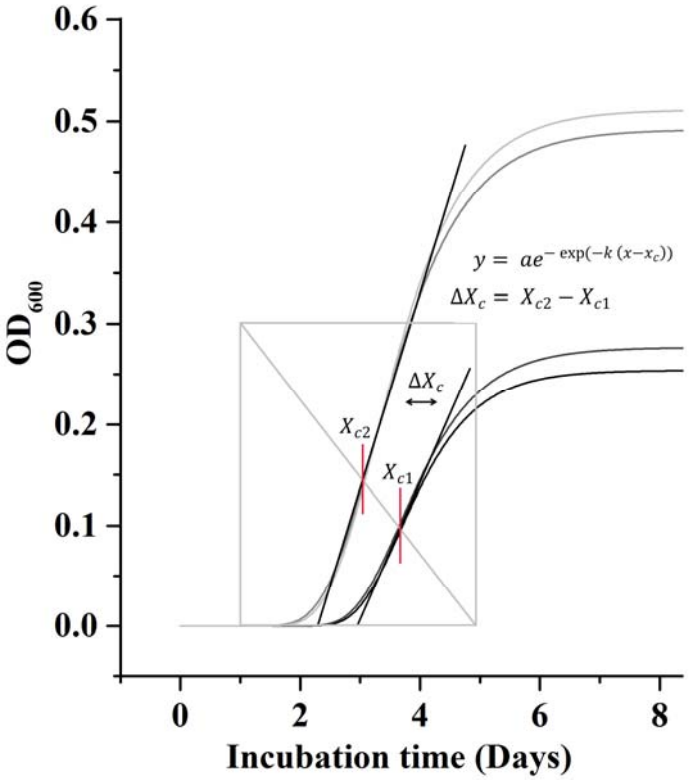

Figure 1.

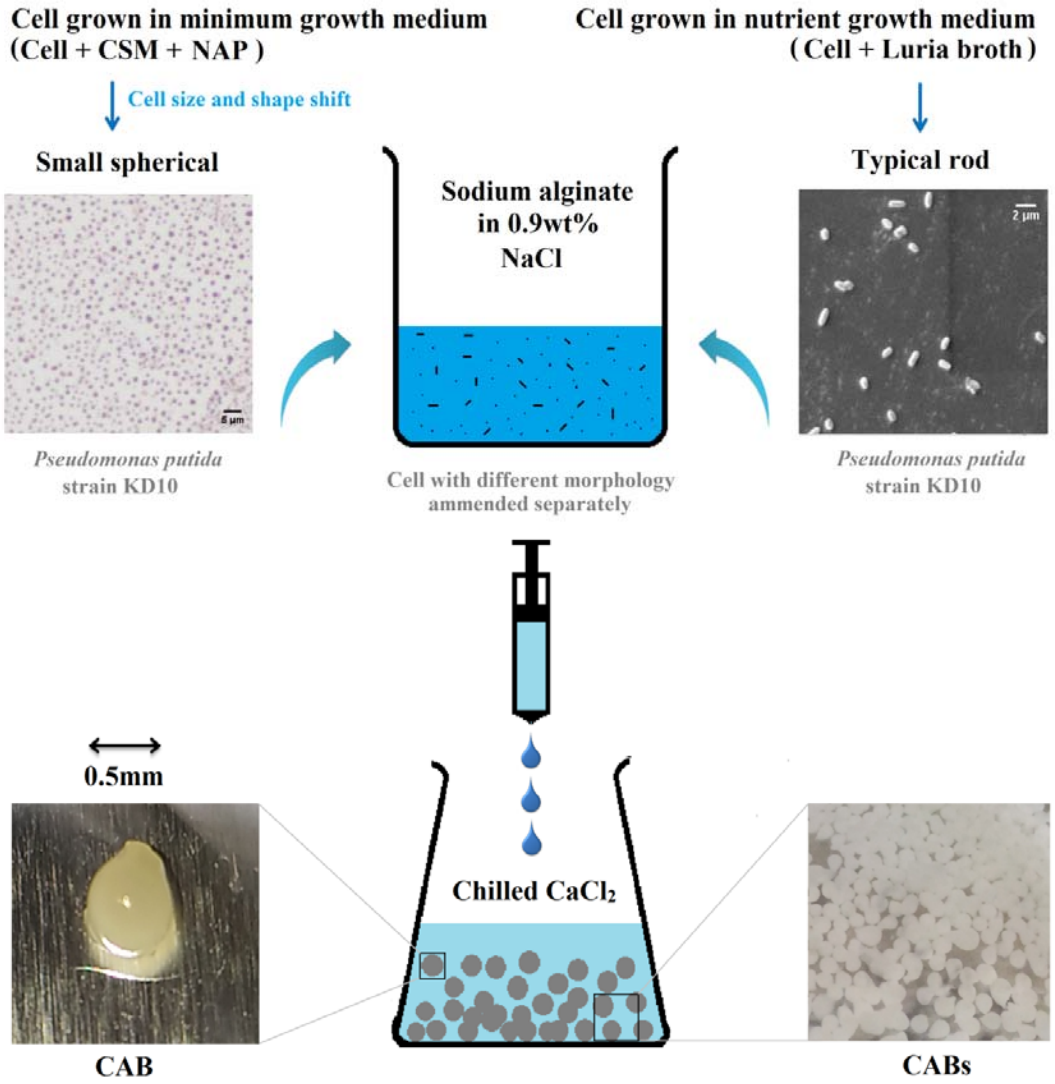

977

978 **Figure 2.**

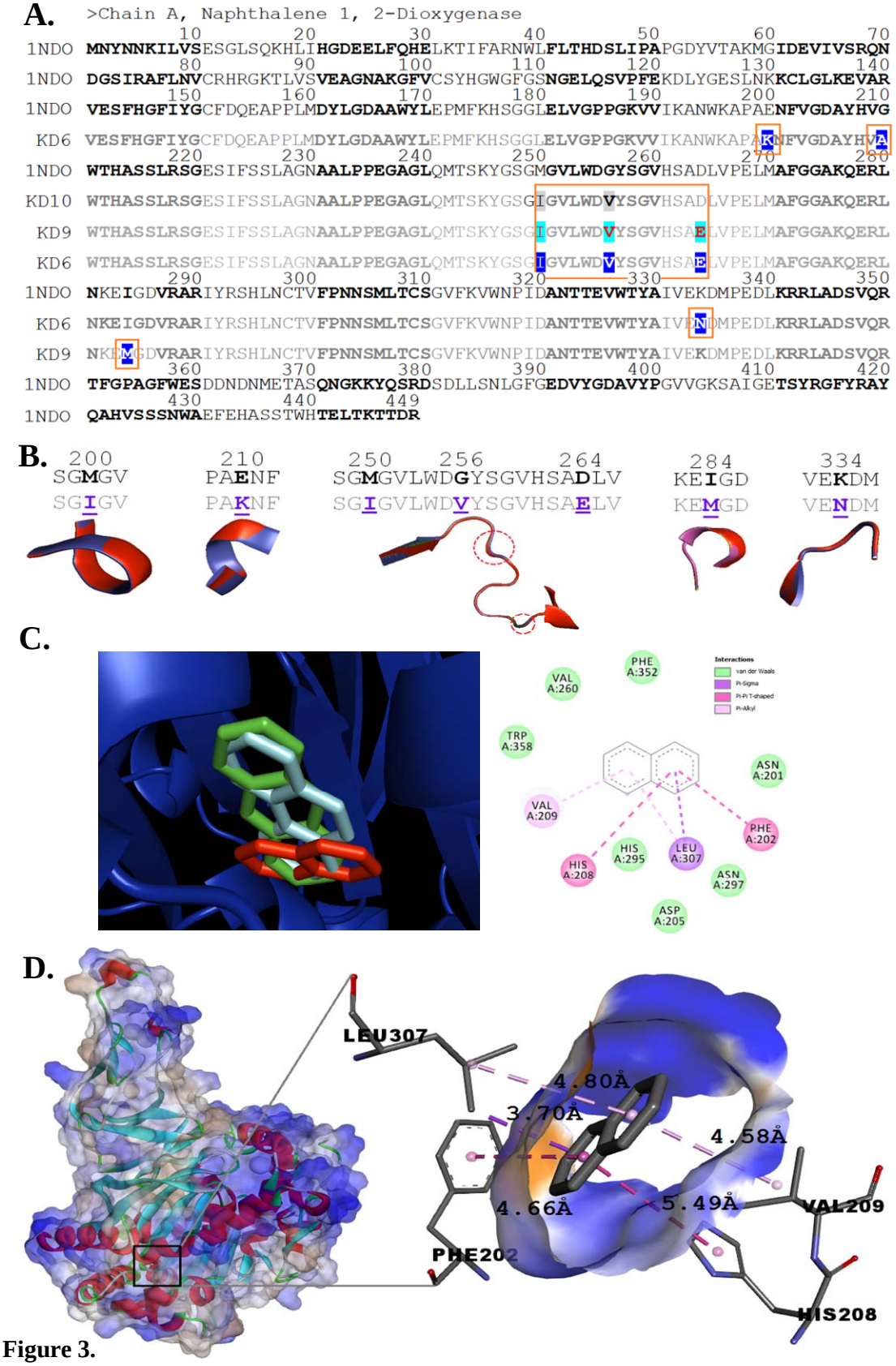

979 **Figure 3.**

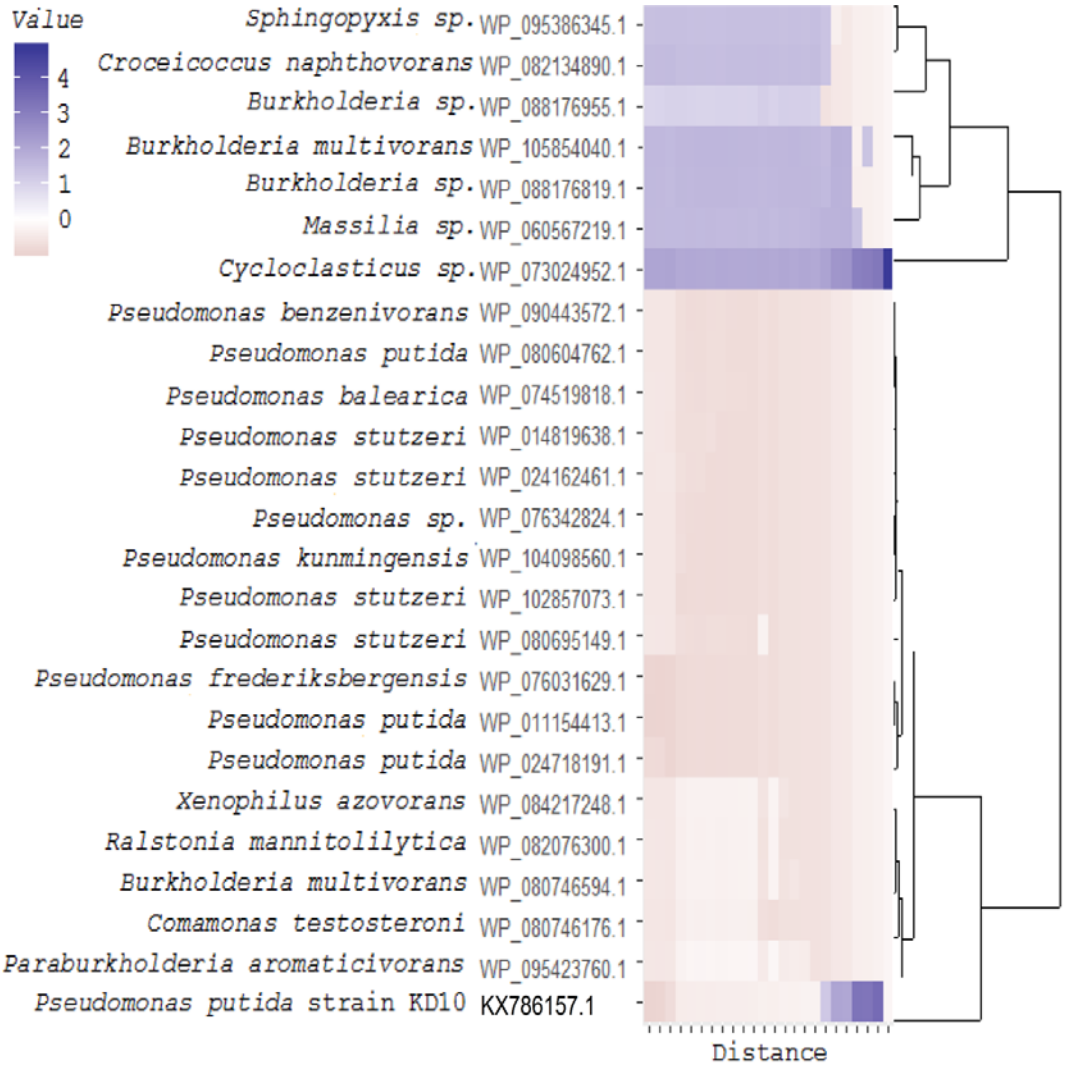

Figure 4.

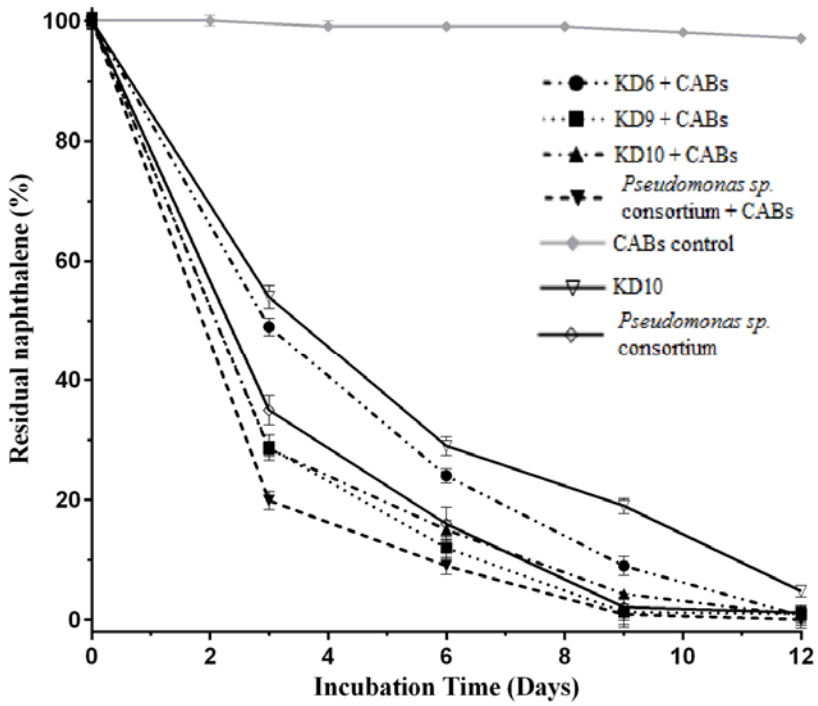

Figure 5.

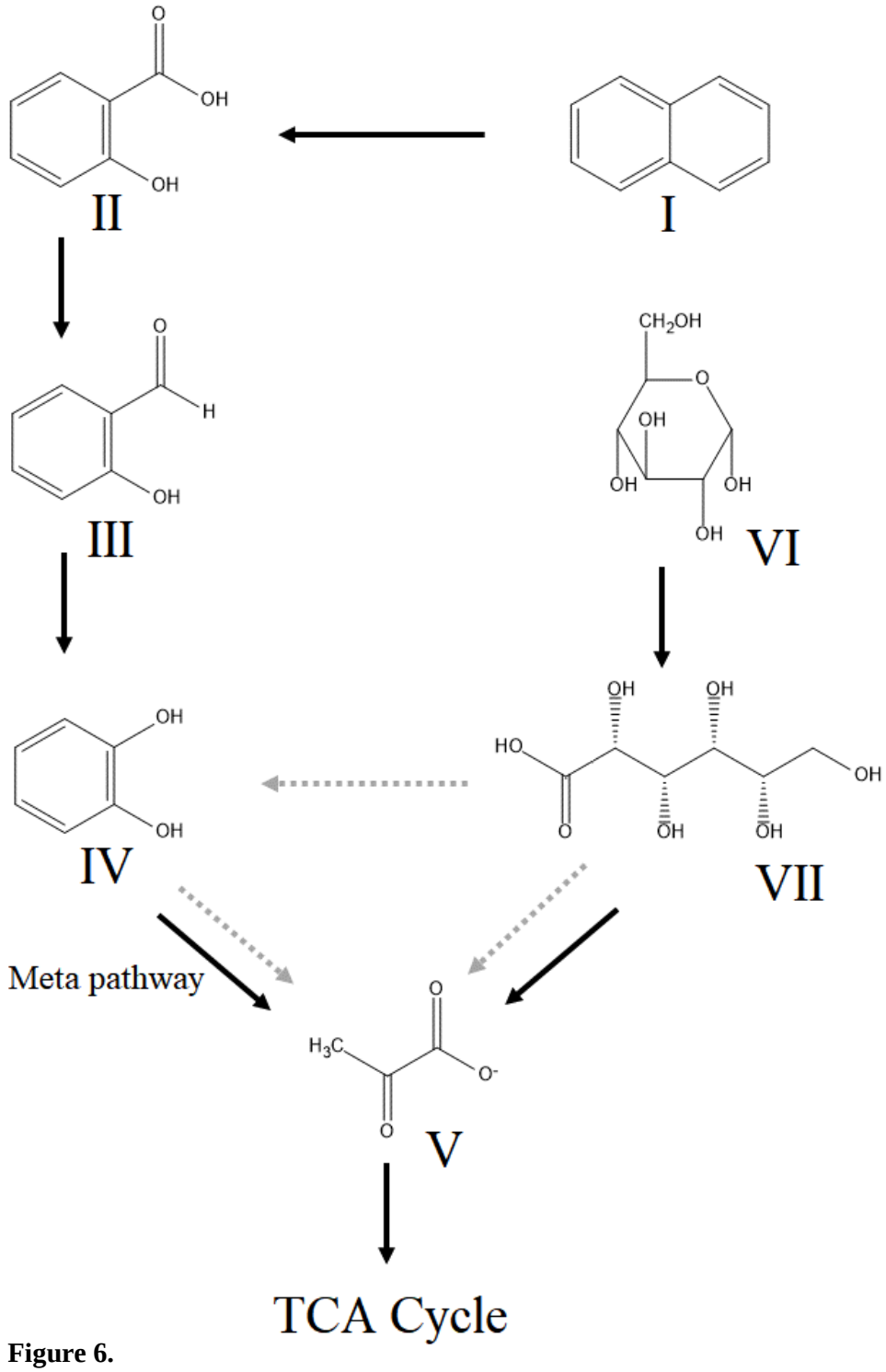

1017 **Figure 6.**